Journal of Molecular Medicine (2025) 103:531–545
https://doi.org/10.1007/s00109-025-02535-y

JMolMed

ORIGINAL ARTICLE

Hepatic microtubule destabilization facilitates liver fibrosis in the mouse model of Wilson disease

Som Dev[1,2] · **Yixuan Dong**[2] · **James P. Hamilton**[2,3]

Received: 29 November 2024 / Revised: 24 February 2025 / Accepted: 18 March 2025 / Published online: 26 March 2025

Abstract

Wilson disease (WD) is a potentially fatal metabolic disorder caused by the inactivation of the copper (Cu) transporter ATP7B, resulting in systemic Cu overload and fibroinflammatory liver disease. The molecular mechanism and effects of elevated Cu on cytoskeletal dynamics in liver fibrogenesis are not clear. Here, we tested the regulation of hepatic cytoskeleton and fibrogenesis with respect to Cu overload in WD. *Atp7b*$^{-/-}$ (knockout) mice with established liver disease, hepatocyte-specific *Atp7b*Δ^{Hep} knockout mice without fibroinflammatory disease, and the age-and sex-matched controls were compared using Western blotting, real-time quantitative reverse transcription PCR (qRT-PCR), immunohistochemical (IHC) staining and transcriptomics (RNA-sequencing) analysis. In *Atp7b*$^{-/-}$ mice with developed liver disease, there is a significant increase in cytoskeletal protein expression with a reduction in α-tubulin acetylation. In these mice before the onset of liver pathology, no significant changes in cytoskeletal nor hepatic stellate cell activation are observed. As hepatic copper levels rise, an increase in cytoskeletal proteins with a decrease in acetylated-α-tubulin/α-tubulin ratio occurs. RNA-sequencing, qRT-PCR, and immunostaining confirm that the tubulin is upregulated at the transcriptional level and hepatocytes are the primary source of early tubulin increases before fibrosis. An increase in α-tubulin with a decrease in α-tubulin acetylation via Hdac6 and Sirt2 induction facilitates fibrosis as reflected by concomitant increases in desmin and α-SMA immunostaining in *Atp7b*$^{-/-}$ mice at 20 weeks. Moreover, strongly positive correlations between α-tubulin and α-tubulin deacetylase with the expression of liver fibrosis markers are observed in animal and human WD. Hepatocyte-specific *Atp7b*Δ^{Hep} mice lack significant changes in tubulin as well as fibrosis despite hepatic steatosis. This study provides evidence that microtubule destabilization causes cytoskeletal rearrangement and facilitates hepatic stellate cell (HSC) activation and fibrosis in the murine model of WD.

Key Messages

- Hepatic cytoskeleton system is induced in Wilson disease.
- Hepatic microtubules acetylation is dysregulated in murine Wilson disease.
- Microtubules destabilization is positively associated with liver fibrosis in Wilson disease.
- Microtubules destabilization concomitant with fibrogenesis exacerbates WD progression.

Keywords Copper · Atp7b · Fibrosis · Wilson disease · Tubulin stability · Microtubules

Abbreviations

Ac-α-tubulin	Acetylated-α-tubulin
ATP7B	ATPase Cu transporting beta
Atp7b$^{-/-}$	Atp7b knockout mice
Atp7bΔ^{Hep}	Hepatocyte-specific Atp7b knockout mice
CBB	Coomassie brilliant blue
Des	Desmin
HSC	Hepatic stellate cell
MTs	Microtubules
mRNA	Messenger RNA
PTM	Post-translational modification
qRT-PCR	Quantitative reverse transcription PCR

✉ Som Dev
som.biochem@aiimskalyani.edu.in

[1] Department of Biochemistry, All India Institute of Medical Sciences, Kalyani, West Bengal 741245, India

[2] Department of Physiology, Johns Hopkins University, School of Medicine, Baltimore, MD, USA

[3] Division of Gastroenterology and Hepatology, Johns Hopkins University, School of Medicine, 725 North Wolfe St, Baltimore, MD 21205, USA

RNA-seq	RNA-sequencing
α-SMA	α-Smooth muscle actin
WD	Wilson disease

Introduction

Hepatic fibrosis is a frequent complication of chronic liver diseases thereby representing a high health and economic burden. Fibrosis can evolve into more severe consequences such as irreversible cirrhosis and hepatocellular carcinoma [1]. Wilson disease (WD) is caused by mutations of the copper transporter ATP7B. It is characterized by the clinical presentation of hepatic copper (Cu) accumulation, inflammation, and fibrosis, potentially causing cirrhosis and death [2, 3]. A better understanding of WD pathogenesis may lead to the development of alternative or supplemental approaches to current therapy. The mechanisms by which elevated Cu triggers hepatic fibroinflammatory disease incompletely defined and whether the hepatic cytoskeleton is involved in this pathogenic transition is unclear. Genetically engineered *Atp7b*$^{-/-}$ mice are a valuable model that recapitulate the human Wilson disease phenotype. Cu accumulation starts before fibroinflammatory disease in *Atp7b*$^{-/-}$ mice [4]. Thus, an understanding of fibrogenic mechanisms is essential to help decelerate disease progression and increase the probability of regression.

Activation of hepatic stellate cells (HSCs) from a resting state is essential for liver fibrinogenesis. HSC activation is characterized by increased profibrogenic cytokines, collagen production, and extracellular matrix formation [5, 6]. As an activated HSC transforms from a quiescent state, extension of cytoplasmic processes occurs. Thus, cellular dynamics may require the involvement of cytoskeletal proteins to facilitate changes in cellular morphology characteristic of HSC activation. The major constituents of the cytoskeleton are microtubules and actin filaments. Previous studies indicate that actin cytoskeleton dynamics participate in HSC activation in vitro in HSC-T6 cells [7] and in primary HSC isolated from fibrotic rat liver [8]. Microtubules (MTs) are polymers of α/β-tubulin heterodimers that comprise the microtubule building block [9]. α-Tubulin acetylation, a post-translational modification (PTM) of the lysine residue at position K40 found in the lumen of the microtubule, is important for the stabilization of MTs. The remainder of the PTMs occur on the outer surface of the microtubule. [9, 10]. Modification of K40 is carried out by α-tubulin acetylase [11] and deacetylases under the regulation of Hdac6 [12] and Sirt2 [13]. Stabilization of MTs via α-tubulin acetylation, is essential for cytoplasmic reorganization, cellular division and differentiation, and intracellular cargo trafficking. For example, stabilization of MTs reduces fibrotic scarring after spinal cord injury in rodents via various mechanisms including decreased transforming growth factor-β (TGF-β) signaling [14]. Loss of α-tubulin acetylation is associated with TGF-β induced epithelial-mesenchymal transition (EMT) in vitro in epithelial cells [15]. These studies suggest that MTs stability may play an important role in the pathogenesis of fibrosis.

Cu excess can impair the dendritic cytoskeleton in hippocampal neurons [16], and kinesin-mediated cargo transport in the brain and other tissues [17]. Earlier reports also found an interplay between Cu and MT cytoskeleton via dynactin 4. Dynactin 4 (p62) is a component of the MT-associated dynactin motor complex that interacts with ATP7B to regulate its Cu-dependent trafficking [18, 19]. Indeed, elevated intracellular Cu contributes to kidney fibrosis by activating lysyl oxidase-mediated matrix crosslinking [20]. Previously, we demonstrated that Cu-induced oxidative stress and cytokines induce liver fibrosis in murine WD via TGF-β and other signaling pathways [3]. However, there is little information known about the role of the MTs cytoskeleton (essential for cytoskeletal reorganization) in the pathogenesis of WD. To address this question, we used *Atp7b*$^{-/-}$ mice and found that these mice with established liver disease, there is a significant increase in cytoskeletal α-tubulin, acetylated α-tubulin, and β-actin protein expression with a decrease in Ac-α-Tub/α-Tub ratio at 20-weeks. These increases in cytoskeleton proteins occur in an age-dependent fashion. Before the onset of liver pathology, no significant changes in cytoskeletal and fibrotic markers were observed whereas at 20 weeks in *Atp7b*$^{-/-}$ mice and patients with WD, induction of microtubule and fibrotic markers were positively correlated at protein and RNA levels. We also found that tubulin induction with a decrease in intraluminal acetylation mediates fibrotic transition in the WD liver. Furthermore, in vivo deletion of Atp7b only in hepatocytes lacks changes in tubulin and fibrosis despite hepatic steatosis. We conclude that dysregulation of MTs is a crucial step that facilitates liver fibrosis in the murine model of WD.

Materials and methods

Animal experiments

Animals were housed at the Johns Hopkins University, School of Medicine (JHUSOM) animal care facility, and the studies followed the National Institutes of Health (NIH) guidelines. Animal protocols were approved by the Institutional Animal Care and Use Committee (IACUC, Protocol number M017MB385). All experimental procedures were carried out on global Atp7b knockout mice: *Atp7b*$^{-/-}$ (KO), *Atp7b*$^{+/-}$(Het) mice of C57BL/6 J (B6), C57BL/6 × 129S6/SvEv (hybrid) background and hepatocyte-specific Atp7b knockout (*Atp7b*$^{\Delta Hep}$), floxed (*Atp7b*$^{Lox/Lox}$) mice of B6 background respectively [21]. The same animal background i.e.

C57BL/6 (global and hepatocyte-specific Atp7b knockout) mice were used for the experiments in the manuscript except for RNA-sequencing done in KO mice on a hybrid background. Each litter was kept in a separate cage; different cages were located in the same room, on the same rack. The control age- and sex-matched animals were either wild-type or heterozygous, knockout and floxed mice on the respective genetic backgrounds. Sex group distribution, genotype, and body weights of $Atp7b^{-/-}$ and $Atp7b^{\Delta Hep}$ mice (B6 background) are detailed in Table S1 and S2 respectively. Mice were euthanized using isoflurane at ages 6 to 45 weeks. Sections of mouse liver were immersed in RNA later (Invitrogen) for qRT-PCR. Tissues were flash-frozen and stored at -80^0C until required and pieces of liver tissues were paraformaldehyde and formalin fixed overnight for OCT and paraffin embedding, respectively.

Human experiment

Liver sections were received from WD patients who underwent liver transplantation for acute or chronic liver failure. Control specimens were obtained from patients who underwent liver resections for other clinical reasons with approved consent [22; U. Leipzig Reg. #236–2006; U. Heidelberg Reg. #346/2005]. Liver sections were flash-frozen in liquid nitrogen and stored for microarray analysis.

Western blotting

Liver tissue (~50 mg) was homogenized with 500 µl RIPA buffer (Sigma), 1X protease, and phosphatase inhibitors (Roche). Protein concentration was estimated by BCA using bovine serum albumin standard. Protein lysates (80–100 µg) were separated on 10% SDS-PAGE gel (Bio-Rad) and transferred using a Trans-blot turbo system (Bio-Rad). After blocking with 5% fat-free milk for 1 h, membranes were incubated with primary antibodies: acetylated α-tubulin (Rabbit monoclonal #5335 T), α-tubulin (Rabbit polyclonal #2144) and β-Actin (Mouse monoclonal #NB600-501) overnight at 4^0C on a shaker, followed by a secondary antibody (anti-rabbit HRP, anti-mouse HRP from Cell Signaling) for 1 h at RT and visualized using Amersham™ Imager 600 (GE). Coomassie brilliant blue (CBB) stained membranes were used for the normalization of target protein expression using ImageJ owing to endogenous loading controls induction. Antibodies' source and dilutions are given in **Table S3**.

RNA Isolation and qRT-PCR

Total liver RNA was isolated from 20–30 mg liver tissue using the QIAshredder and RNeasy Mini Kit (Qiagen) following manufacturers' protocol. First-strand cDNA was synthesized from 1 µg RNA (quantified by IMPLEN Nano photometer) using the High Capacity RNA-to-cDNA Kit (Applied Biosystems). PCR reactions were performed with 2X PowerUp SYBR Green Master Mix and 5 µl of cDNA (1:5 diluted) on the QuantStudio6 Flex system (Applied Biosystems) using primers described in **Table S4**. The transcript abundances were determined using a relative quantitative *CT* method [23] and Rpl19 was used as an endogenous control.

Transcriptomics data analysis

RNA-sequencing data was generated from the $Atp7b^{+/-}$(Het), and $Atp7b^{-/-}$ (KO) of C57BL/6 × 129S6/SvEv (hybrid) background liver RNA samples with RIN value of 8 or higher [3]. Libraries were generated (TrueSeq Stranded Total RNA library) and the sequencing was performed by Psomagen Inc, Rockville, MD, using Illumina NovaSeq6000 (150 bp, paired-end). Expression profiles were represented as read count and FPKM (Fragments Per Kilobase of transcript per Million mapped reads) values. Data are available in the Gene Expression Omnibus database under accession number GSE174015. Data visualization of cytoskeletal transcripts was done using SRplot [24]. Relative gene expression of tubulin regulatory enzymes, microtubule-associated proteins and EMT biomarkers were done using transcript per million (TPM) values of KO as compared to Het control.

Microarray analysis

Microarray (Affymetrix) data was generated from the WD patients (liver sections) who underwent liver transplantation for acute or chronic liver failure. Control specimens were obtained from patients who underwent liver resections for other clinical reasons [22]. RNA was isolated using TRIzol followed by RNeasy clean-up (Qiagen). RNA integrity of samples (eight biological replicates for control liver and eight for WD patients) was examined on an Agilent 2100 Bioanalyzer using the RNA 6.000 LabChip Kit (Agilent Technologies). Microarray processing was performed using third-generation Affymetrix GeneChip Scanner 3000. Data analysis was performed using Partek software. Data is submitted in the Gene Expression Omnibus database under accession number GSE197406.

Immunofluorescence

Liver pieces were fixed (4% paraformaldehyde), cryosectioned (7–10 µm), and stained with anti-tubulin (Rat monoclonal #ab6160), anti-desmin (Rabbit monoclonal #ab32362), anti-SMA (Rabbit monoclonal #ab32362) and anti-albumin (Goat polyclonal #NB600-41532) antibodies as detailed in the **Table S3**. Images were acquired by using LSM800 confocal laser microscope. TIFF files were

imported into Adobe Photoshop, and the entire field was enhanced and sharpened by using the levels command.

Immunohistochemistry

Liver tissue pieces were fixed (10% formalin), processed, embedded (paraffin), and cut at the Johns Hopkins Pathology Core. Sections undergo antigen retrieval (GTX 30396; Citrate buffer, pH-6.0), blocking (normal goat serum), staining with anti-tubulin (ab6160; 1:250) overnight at 4^0C followed by biotinylated secondary antibody (BP9400; 1:1000) incubation for 1 h at RT and developed using ABC reagent (PK-4000) and DAB (BD-550880). Sections were counterstained with hematoxylin (14166S). Images were acquired using an Olympus light color microscope.

Statistics

Statistical analysis was performed using Prism 10 (GraphPad). Results are presented as mean ± SD unless otherwise stated. Students t-test, two-tailed t-test, and ANOVA were used for analysis. Correlation between tubulin and fibrotic markers, tubulin (de)acetylases, and fibrotic markers were analyzed using Pearson's correlation and linear regression. Pearson correlation coefficient (r) and p-value were calculated using Prism 10. P-value < 0.05 was considered significant.

Results

Cytoskeleton proteins are upregulated in Atp7b$^{-/-}$ mice while microtubule acetylation is decreased

Our previous studies demonstrated activation of HSC associated with collagen production and extracellular matrix formation in murine WD [3, 22]. To better understand the role of the cytoskeleton in WD pathology we first performed Western blotting of liver tissue homogenates from control *Atp7b*$^{+/-}$ animals, which do not have liver disease, and *Atp7b*$^{-/-}$ animals when their liver disease is fully established at 20 weeks after birth [4]. We observed a significant increase in α-tubulin (fourfold) and β-actin (4.2-fold) proteins in KO liver as compared to Het control at 20 weeks (Fig. 1A). Increases in α-tubulin protein abundance may also increase post-translational modification (PTM) such as acetylation, essential for microtubules (MTs) function. Accordingly, an abundance of acetylated α-tubulin was found higher (5.96-fold) in the KO liver as compared to Het (Fig. 1A-B). These results suggest that the cytoskeleton system is induced in a murine model of WD.

Acetylated α-tubulin is a marker of stable MTs. To test the mechanism of MTs stabilization and cytoskeletal dynamics, first, we immunoblotted for α-tubulin and acetylated α-tubulin simultaneously. There was a significant increase in α-tubulin and acetylated α-tubulin suggesting increased tubulin mass and stability, however, there was about ~ 40% decrease in α-tubulin acetylation when normalized to total α-tubulin in KO mice compared to Het (Fig. 1C) which is potentially due to higher acetylated α-tubulin (2.5-fold) expression than α-tubulin in Het control samples (Fig. 1A, left side Het panels). To test how early cytoskeletal system is induced and microtubule acetylation is affected, we analyzed *Atp7b*$^{-/-}$ mice liver samples from 6-, 12-, and 20-weeks age groups. Results suggest that cytoskeletal proteins: α-tubulin (2 to fivefold), acetylated α-tubulin (2.8 to 9.6-fold), and β-actin (3.4 to 16-fold) protein expression is induced whereas α-tubulin acetylation (Ac-α-tubulin/α-tubulin ratio) decreased ~ 27–47% from 12 to 20 weeks as compared to 6 weeks *Atp7b*$^{-/-}$ mice in age-dependent manner (Fig. 1D-F). However, changes in cytoskeletal proteins and the Ac-α-tubulin/α-tubulin ratio were not statistically significant at 12 weeks versus 6 weeks in the *Atp7b*$^{-/-}$ mice. Taken together, these results suggest that in *Atp7b*$^{-/-}$ mice with established liver disease (20 weeks after birth) cytoskeleton system is induced with a significant decrease in MTs acetylation.

Tubulin is induced in Atp7b$^{-/-}$ mice but not in Atp7b△^{Hep} without liver fibrosis

To understand whether the increase in total α-tubulin and decrease in α-tubulin acetylation is unique to *Atp7b*$^{-/-}$ mice, and if is there a similar phenomenon in hepatocyte-specific *Atp7b*△^{Hep} mice, we performed immunoblot analysis. Targeted inactivation of Atp7b in hepatocytes causes hepatic Cu accumulation and steatosis without fibrosis [25]. Before the development of steatosis or other liver injury, there were no significant changes in α-tubulin, acetylated α-tubulin, and β-actin protein levels in *Atp7b*$^{-/-}$ and *Atp7b*△^{Hep} mice at 6 weeks (Fig. 2A-C). This data suggests that the cytoskeleton system is not altered in *Atp7b*$^{-/-}$ and *Atp7b*△^{Hep} mice at an early age despite copper accumulation. Furthermore, total α-tubulin was also not significantly altered in *Atp7b*△^{Hep} mice even at 20 weeks. Tubulin and acetylated α-tubulin expression were induced in KO mice as compared to Het whereas a decrease in α-tubulin acetylation (Ac-α-Tub/α-Tub) occurs significantly in KO (~ 78%) and *Atp7b*△^{Hep} mice (~ 48%) at 20-weeks (Fig. 2D-F). We next explored tubulin and fibrotic markers in *Atp7b*△^{Hep} mice at 45 weeks by qRT-PCR. There was no change in α-tubulin, β-tubulin (Tub1a1, Tubb1), and fibrotic markers (Col1a1, Timp1) mRNA levels observed in *Atp7b*△^{Hep} mice even at older age (Fig. 2G). More than ~ 99% reduction in Atp7b mRNA

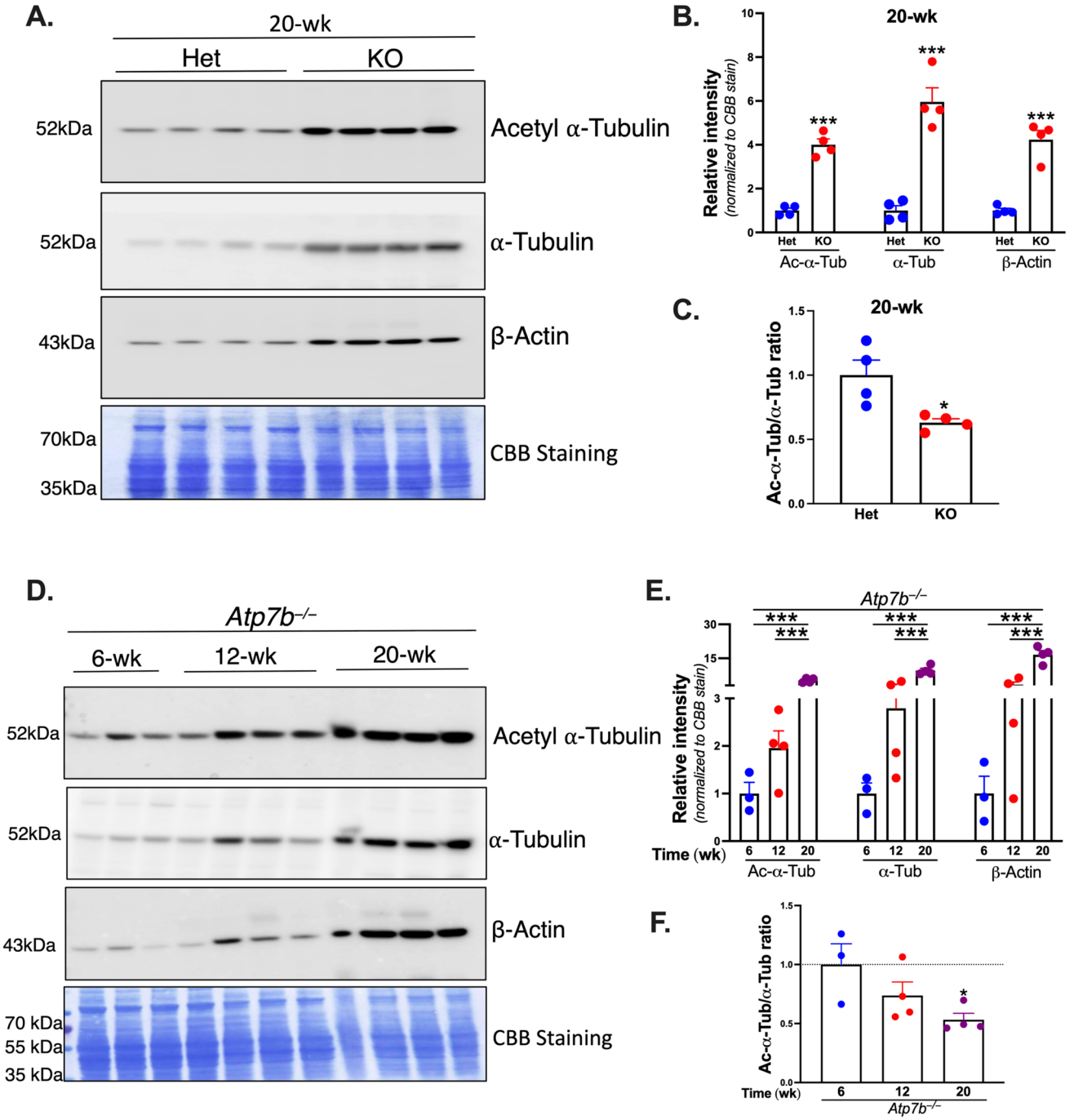

Fig. 1 Cytoskeleton system induced in *Atp7b*$^{-/-}$ mice with decreased α-tubulin acetylation. **A.** Liver tissue lysates from *Atp7b*$^{+/-}$ (Het) and *Atp7b*$^{-/-}$ (KO) mice of C57BL/6 (B6) background were immunoblotted with acetylated α-tubulin, α-tubulin, β-actin specific antibodies, and membrane stained with Coomassie brilliant blue (CBB; n = 4 mice/group, 20 weeks). Each lane represents an individual mice sample. **B.** Densitometry of the cytoskeletal proteins was performed and normalized with CBB stain using image J. **C.** Acetylated α-tubulin/α-tubulin levels were significantly reduced in KO liver compared to Het control at 20 weeks. **D.** Cytoskeleton proteins are induced in an age-dependent manner. Liver tissue lysates from *Atp7b*$^{-/-}$ mice were immunoblotted with acetylated α-tubulin, α-tubulin, and β-actin antibodies (n = 3–4 mice/age group). **E.** Relative quantification of cytoskeletal proteins with CBB stain was performed in *Atp7b*$^{-/-}$ mice from 6–20 weeks. **F.** Acetylated α-tubulin/α-tubulin ratio was reduced with age in *Atp7b*$^{-/-}$ mice at 12 and 20 weeks compared to 6-week-old *Atp7b*$^{-/-}$ mice. Value represents mean ± SD. **P = 0.05, **P = 0.01, ***P = 0.001* between KO vs Het; KO mice in different age groups

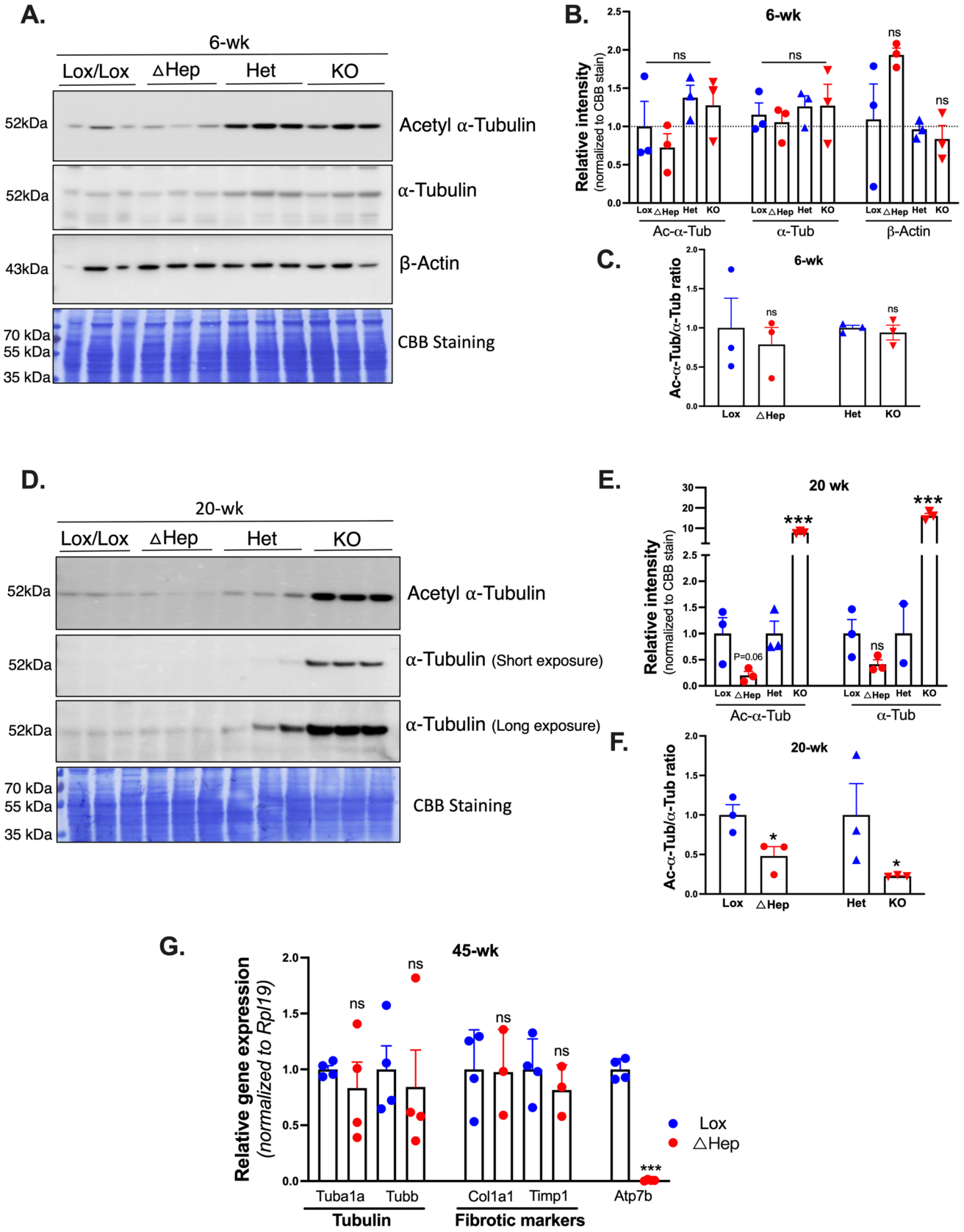
A.
6-wk
Lox/Lox
ΔHep
Het
KO
52kDa
Acetyl α-Tubulin
52kDa
α-Tubulin
43kDa
β-Actin
70 kDa
55 kDa
35 kDa
CBB Staining
B.
6-wk
Relative intensity
(normalized to CBB stain)
ns
Lox ΔHep Het KO
Ac-α-Tub
α-Tub
β-Actin
C.
6-wk
Ac-α-Tub/α-Tub ratio
Lox
ΔHep
Het
KO
D.
20-wk
Lox/Lox
ΔHep
Het
KO
52kDa
Acetyl α-Tubulin
α-Tubulin (Short exposure)
α-Tubulin (Long exposure)
70 kDa
55 kDa
35 kDa
CBB Staining
E.
20 wk
***
P=0.06
Relative intensity
(normalized to CBB stain)
Ac-α-Tub
α-Tub
F.
20-wk
Ac-α-Tub/α-Tub ratio
*
Lox
ΔHep
Het
KO
G.
45-wk
Relative gene expression
(normalized to Rpl19)
Tuba1a
Tubb
Col1a1
Timp1
Atp7b
Tubulin
Fibrotic markers
Lox
ΔHep

◂**Fig. 2** Tubulin is induced in $Atp7b^{-/-}$ mice but not in $Atp7b\Delta^{Hep}$ without liver disease. **A-B.** Liver tissue lysates from $Atp7b^{Lox/Lox}$, $Atp7b^{\Delta Hep}$, $Atp7b^{+/-}$ (Het) & $Atp7b^{-/-}$ (KO) mice at 6 week-old (n = 3 mice/group from B6 background) were immunoblotted with acetylated α-tubulin, α-tubulin and β-Actin specific antibodies. No change in cytoskeletal proteins was observed in $Atp7b^{\Delta Hep}$ and KO mice at 6 weeks. Cytoskeletal proteins were normalized with CBB stain **C.** Acetylated α-tubulin/α-tubulin ratio was unaltered at 6 weeks in $Atp7b^{\Delta Hep}$ and KO mice. **D-E.** Acetylated α-tubulin and α-tubulin were significantly induced in KO mice as compared to Het whereas acetyl α-tubulin was reduced in $Atp7b^{\Delta Hep}$ as compared to lox control at 20 weeks. α-tubulin was not significantly changed in $Atp7b^{\Delta Hep}$ mice compared to lox. **F.** Acetylated α-tubulin/α-tubulin ratio was significantly reduced in both KO and $Atp7b^{\Delta Hep}$ mice as compared to respective controls. **G.** qRT-PCR analysis demonstrates no change in tubulin (Tub1a1, Tub1b1) and fibrotic markers (Col1a1, Timp1) mRNA levels in $Atp7b^{\Delta Hep}$ mice liver at 45 weeks. Atp7b mRNA was more than 99% reduced in $Atp7b^{\Delta Hep}$ mice as compared to floxed control. Results were normalized to Rpl19. (n = 4 male mice/group). Value represents mean ± SD. $*P = 0.05$, $**P = 0.01$, $***P = 0.001$ between KO vs Het; Atp7b$^{\Delta Hep}$ vs Lox mice respectively; ns, nonsignificant

expression confirms the deletion of Atp7b in $Atp7b\Delta^{Hep}$ mice compared to the floxed control (Fig. 2G). At the same time, Cu storage (metallothionein) and lipid (fatty acid synthase) genes were significantly upregulated in $Atp7b\Delta^{Hep}$ mice **(Suppl. Figure 1)** indicating Cu accumulation and steatosis. All these results demonstrate that tubulin is induced in $Atp7b^{-/-}$ but not in $Atp7b\Delta^{Hep}$ mice without liver fibrosis.

Tubulin induction occurs at the transcriptional level & hepatocyte is the main source of tubulin induction

To determine the mechanism of tubulin induction and whether tubulin is regulated only at translation and post-translational (acetylation) levels, we initially examined a bulk RNA-sequencing dataset from $Atp7b^{-/-}$ mice liver. There was a significant upregulation in α-tubulin, β-tubulin family transcripts, and actin in KO mice as compared to Het control at 20 weeks (Fig. 3A). We further confirmed α-tubulin and β-tubulin mRNA expression by qRT-PCR. There was a significant increase in Tub1a1 (~ 2.4-fold) and Tubb1 (~ 2.45-fold) mRNA levels in KO mice liver (Fig. 3B). Both these results suggest that tubulin expression is regulated at the transcriptional level.

To investigate the cellular source of tubulin induction in $Atp7b^{-/-}$ mice liver, we performed immunostaining on frozen liver sections using specific anti-α-tubulin (monoclonal) and observed under a confocal microscope. There was an increase in α-tubulin immunostaining in $Atp7b^{-/-}$ mice liver as compared to wild-type (WT) mice at 7 weeks. However, albumin (hepatocyte marker) staining was reduced in KO as compared to WT (Fig. 3C). Since hepatocytes are parenchymal liver cells that constitute the bulk of liver mass, these data demonstrate that tubulin and albumin expression is inversely regulated in $Atp7b^{-/-}$ mice, and hepatocytes are the primary source of tubulin expression. We further examined α-tubulin by immunohistochemistry. Immunohistochemical analysis of $Atp7b^{-/-}$ mouse liver tissue revealed strong α-tubulin staining in $Atp7b^{-/-}$ hepatocytes and non-parenchymal liver cells as compared to Het at 20 weeks (Fig. 3D). However, α-tubulin staining in ballooned (enlarged) hepatocytes was less intense compared to adjacent hepatocytes reflecting an altered cytoskeleton.

Tubulin induction with a decrease in α-tubulin acetylation facilitates HSC activation

To understand the role of tubulin induction in fibrosis, we performed co-immunostaining of tubulin with fibrotic markers. Activation of HSCs is an important hallmark of liver fibrosis and desmin is a marker of stellate cells. At 7 weeks, there was no change in desmin, however, there was an apparent increase in α-tubulin immunostaining observed in KO compared to WT mice. (Fig. 4A**).** This result demonstrates that α-tubulin induction starts before fibrotic changes in the KO liver. Tubulin was colocalized with desmin in HSCs irrespective of the genotype. At 20 weeks, there was a massive induction in both desmin as well as α-tubulin immunosignal in KO mice (Fig. 4B). There were significant changes in hepatocyte morphology at 20 weeks as well. We also performed α-tubulin co-immunostaining with α-smooth muscle actin (SMA). SMA is another well-known marker of activated HSCs [26]. We observed a similar phenomenon. There was a substantial induction in SMA along with α-tubulin at 20 weeks **(Suppl. Figure 2)**. All these results suggest that an increase in tubulin expression correlated with fibrotic changes in $Atp7b^{-/-}$ mice liver at 20 weeks.

Transcriptomic analysis of $Atp7b^{-/-}$ mice (RNA-seq) and WD patients (microarray) liver demonstrated that an increase in the tubulin expression correlated positively with fibrosis. There was a strong positive association between α-tubulin and fibrotic markers such as secreted phosphoprotein 1 (Spp1), collagen 1 alpha 2 (Col1a2), tissue inhibitor of metalloproteinase 1 (Timp1), lysyl oxidase-like 2 (Loxl2), vimentin (Vim) and α-smooth muscle actin (Acta2). A significant positive correlation between Tuba1a and Spp1 ($p < 0.0001$), Tuba1a and Col1a2 ($p = 0.003$), Tuba1a and Timp1 ($p = 0.001$), Tuba1a and Loxl2 ($p < 0.0001$), and Tuba1a and Vim ($p = 0.002$), and Tuba1a and Acta2 ($p = 0.036$) found in $Atp7b^{-/-}$ mice liver at 20 weeks compared to Het control **(Suppl. Figure 3A-F).** Similarly, significant positive correlation between Tuba1a and Spp1 ($p = 0.002$), Tuba1a and Col1a2 ($p = 0.001$), Tuba1a and Timp1 ($p = 0.04$), Tuba1a and Loxl2 ($p = 0.043$), Tuba1a and Vim ($p = 0.05$), and Tuba1a and Acta2 ($p = 0.068$) found in WD patients' liver **(Suppl. Figure 4A-F)**. The most significantly (fold-change) and consistently (p-value) up-regulated transcripts in murine WD and WD patients' liver among

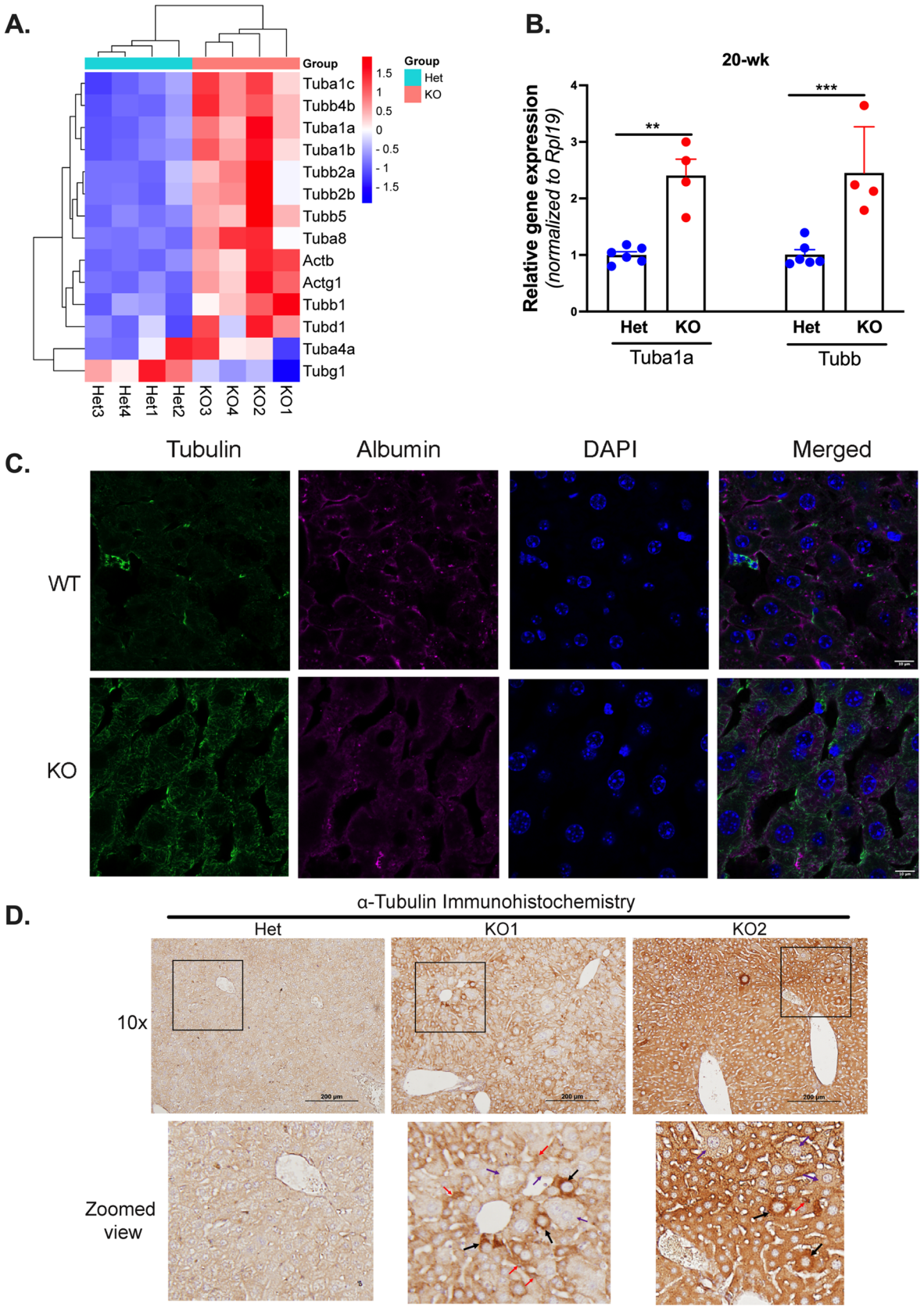
A.
Group
Tuba1c
Tubb4b
Tuba1a
Tuba1b
Tubb2a
Tubb2b
Tubb5
Tuba8
Actb
Actg1
Tubb1
Tubd1
Tuba4a
Tubg1
Het3
Het4
Het1
Het2
KO3
KO4
KO2
KO1
Group
Het
KO
1.5
1
0.5
0
- 0.5
- 1
- 1.5
B.
20-wk
Relative gene expression
(normalized to Rpl19)
**
***
Het
KO
Tuba1a
Het
KO
Tubb
C.
Tubulin
Albumin
DAPI
Merged
WT
KO
D.
α-Tubulin Immunohistochemistry
Het
KO1
KO2
10x
Zoomed
view

◂**Fig. 3** Tubulin induction occurs at the transcriptional level & hepatocyte is the main source of early tubulin induction. *A.* Heatmap analysis of cytoskeletal transcripts was generated using SRplot with row scaling and clustering of transcript abundances in KO mice compared to Het controls at 20 weeks. Positive value in red denotes upregulation, whereas negative value in blue denotes down-regulation (n = 4 male mice/group of C57BL/6 × 129S6/SvEv background). **B.** qRT-PCR analysis demonstrates upregulation of Tub1a1 and Tub1b1 mRNA in KO mice liver at 20 weeks (n = 4–6 female mice/group of B6 background). **C.** Immunostaining of α-tubulin (green) in tissue sections revealed a stronger signal in KO mice liver compared to WT mice at 7 weeks before pathologic onset. Hepatocyte marker albumin (red) expression decreased. DAPI (4',6-diamidino-2-phenylindole; blue) stains nuclei. Scale bar, 10 μm. **D.** Immunohistochemical analysis demonstrates upregulation of α-tubulin protein expression in hepatocytes (black arrow) and non-parenchymal liver cells (red arrow) whereas α-tubulin staining in ballooned hepatocytes (purple arrow) was less compared to adjacent cells indicated in the zoomed view in KO mice at 20 weeks. Scale bar, 200 μm; n = 3 mice/group. Value represents mean ± SD. ***P = 0.01,* ****P = 0.001* between KO vs Het mice

tubulin are Tuba1a, Tuba1b, Tuba1c, Tubb2b, Tubb4b and fibrotic markers Spp1, Col1a2, Timp1, Loxl2, Vim, Acta2, and other cytoskeletal genes (Fig. 4C). All these data suggest that hepatic cytoskeleton changes are essential for liver fibrogenesis in WD irrespective of species and genotype.

Loss of α-tubulin acetylation affects MTs stabilization and causes TGF-β induced EMT [15]. We observed a significant decrease in α-tubulin acetylation in murine WD (Fig. 1C, F **and** Fig. 2F). To determine whether enzymes involved in acetylation and deacetylation are playing a pivotal role in this PTM, we examined their expression in *Atp7b*$^{-/-}$ mice using our RNA-sequencing dataset. There was no significant change in the α-tubulin acetylase Atat1, whereas there was a more than 1.5-fold increase in tubulin deacetylase expression; histone deacetylase 6 (~ 1.65-fold) and sirtuin 2 (~ 1.58-fold) in KO mice compared to Het control at 20 weeks (Fig. 4D). This data suggests that increases in total α-tubulin along with its deacetylases cause decreased Ac-α-Tub/α-Tub level, hence acetylated MTs are reduced in KO mice. Microtubule-associated proteins (MAPs) are important for the stabilization and destabilization of MTs. Significant induction in microtubule destabilizers mRNA expression especially ~ tenfold increase in stathmin 1 (Stmn1 which binds α & β-tubulin dimers and prevents polymerization), ~ 45-fold increase in Kif2c (fraying and depolymerization along the MTs), ~ threefold increase in Eml2 (binds MTs and promotes disassembly). Microtubules severing enzymes such as Katnb1 (2.71 fold) and Katnbl1 (2.4 fold) were also significantly upregulated. On the other hand, there was ~ 1.5–3.5 fold increase in MTs stabilizers (such as Map4, Map7, Mapre1-3, Clip1, Clasp1-2, Camsap1-3) expression observed in KO mice liver as compared to Het control (**Suppl. Figure 5A**). Furthermore, there was a significant increase in MTs motor proteins kinesin and dynein family transcripts in KO liver **(Suppl. Figure 5B**). These results suggest that MAPs are dysregulated and overall hepatic microtubule stability is affected in murine WD.

To strengthen our findings and better understand the relationship of MTs (de)acetylation role in fibrosis, we examined their association between α-tubulin deacetylases and fibrotic markers. There was a significant positive correlation between Hdac6 and Spp1 (p = 0.059), Hdac6 and Col1a2 (p = 0.04), Hdac6 and Timp1 (p = 0.04); Hdac6 and Loxl2 (p = 0.011), and Hdac6 and Vim (p = 0.056) in *Atp7b*$^{-/-}$ mice liver compared to Het control at 20 weeks (Fig. 5A-F). Similar positive associations were observed between Sirt2 and Spp1 (p = 0.014); Sirt2 and Col1a2 (p = 0.014), Sirt2 and Timp1 (p = 0.015); Sirt2 and Loxl2 (p = 0.007); Sirt2 and Vim (p = 0.01), and Sirt2 and Acta2 (p = 0.048) in *Atp7b*$^{-/-}$ mice liver (Fig. 5G-L). On the other hand, there was a non-significant negative correlation between tubulin acetylase Atat1 and fibrotic markers (**Suppl. Figure 6A-F**). These data indicate that MTs destabilization by modulating acetylation is associated with fibrosis. Taken together, impairment of MTs stability leads to hepatic cytoskeleton reorganization and facilitates HSC activation in WD.

Discussion

WD caused by inactivation of ATP7B leads to Cu accumulation that triggers pathomorphological changes in the liver ranging from hepatocyte dysfunction to hepatic stellate cell (HSCs) activation and fibrosis, ultimately causing cirrhosis and death if untreated. Activation of HSCs from a quiescent state is essential for liver fibrogenesis. Hepatic fibrosis is a potentially life-threatening complication associated with chronic liver conditions including WD. Hepatic cytoskeletal dynamics might play an important role in their cellular transformation. The molecular mechanisms of how elevated Cu involves cytoskeletal dynamics in liver fibrogenesis are not clear. In this study, we provide strong evidence of altered cytoskeletal dynamics in WD and the mechanism of tubulin regulation and microtubule destabilization in facilitating HSCs activation and fibrosis in murine WD. We also found a significant positive correlation between microtubule regulation and fibrosis.

We show that in *Atp7b*$^{-/-}$ mice with established liver disease, cytoskeleton proteins are induced with significant upregulation in α-tubulin, acetylated α-tubulin, and β-actin at the translational level. α/β-Tubulin heterodimers are building blocks of microtubules (MTs) and acetylation (post-translational modification, PTM) of α-tubulin in the luminal side results in acetylated MTs which are long-lived and considered stable [9]. This stabilization process is important for MT cytoskeleton dynamics. Here, we identified that despite the increase in total α-tubulin and corresponding acetylated

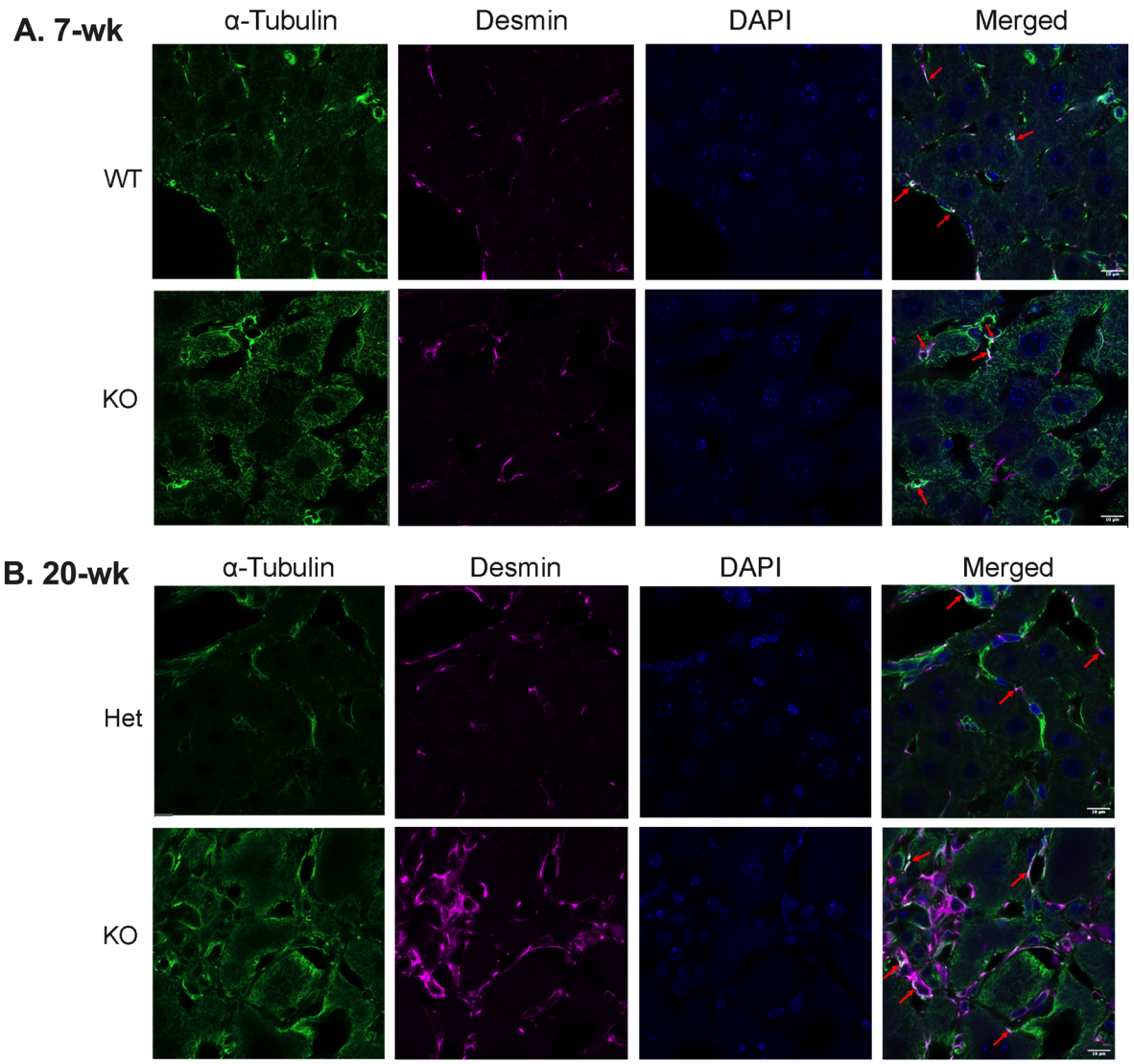

C.

Gene symbol	KO vs Het Relative FC (p-value)	WD vs Normal Relative FC (p-value)
Spp1	7.4 (0.03)	46.6 (7.8E-07)
Col1a2	6.0 (0.04)	9.0 (7.8E-07)
Timp1	4.1 (0.05)	7.0 (2.9E-05)
Loxl2	6.2 (0.01)	2.5 (0.0002)
Vim	6.0 (0.05)	3.3 (0.007)
Tubb2b	4.0 (0.01)	1.3 (0.018)
Tubb4b	3.8 (0.002)	1.93 (0.011)
Actg1	3.7 (0.005)	1.5 (0.03)
Tuba1a	3.0 (0.003)	4.2 (1.8E-05)
Tuba1b	3.2 (0.004)	1.8 (0.011)
Tuba1c	2.8 (0.001)	1.84 (0.01)
Acta2	2.3 (0.2)	3.4 (0.0005)

D.

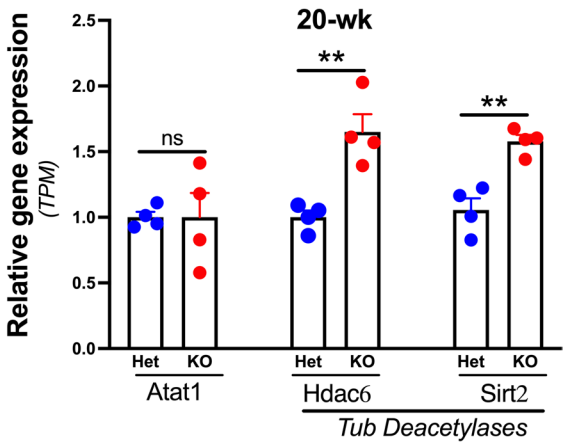

◂**Fig. 4** Tubulin induction with a decrease in α-tubulin acetylation facilitates HSC activation in *Atp7b*$^{-/-}$ mice. **A.** Immunostaining of α-tubulin (green) in tissue sections revealed a stronger signal in KO mice liver compared to WT mice at 7 weeks whereas desmin (red) remains unchanged. DAPI (4',6-diamidino-2-phenylindole; blue) stains nuclei. (n = 3 mice/group of B6 background). **B.** Both α-tubulin and desmin immunosignal intensity is increased in KO mice at 20 weeks as compared to Het mice. DAPI is used as a nuclear marker. Colocalization of α-tubulin and desmin in HSCs indicated by the bright red arrow in KO. Scale bar, 10 µm. (n = 3 mice/group of B6 background). **C.** Most significantly changed cytoskeletal and fibrotic markers in mouse (RNA-seq) and human WD (microarray) dataset; values represent relative fold change, n = 4 male mice/group for KO vs Het; n = 7–8 patients/group for WD vs Normal liver. **D.** Tubulin deacetylases Hdac6 and Sirt2 are significantly induced in KO mice whereas α-tubulin acetylase Atat1 is unaltered (n = 4 male mice/group of C57BL/6 × 129S6/SvEv background). Value represents mean ± SD. ***P = 0.01* between KO vs Het; TPM, Transcript per million; ns, nonsignificant

α-tubulin, the acetylated α-tubulin/α-tubulin protein ratio levels were reduced significantly in *Atp7b*$^{-/-}$ mice liver suggesting reduced acetylated MTs. Also, this decrease in α-tubulin acetylation is exacerbated in advanced murine WD (Fig. 1F).

Understanding the mechanism of tubulin regulation, tubulin expression was examined using RNA-sequencing data. In agreement with sequencing data, tubulin induction was confirmed at the mRNA level by qPCR. Our findings revealed that the increase in cytoskeletal protein expression was due to a higher transcription rate in *Atp7b*$^{-/-}$ mice (Fig. 3). This study suggests that tubulin is regulated at transcriptional as well as post-translational levels. PTM of α-tubulin, especially acetylation/deacetylation, is essential for MTs stabilization [10]. This reaction is carried out by the α-tubulin acetylase Atat1 [11] and deacetylases via Hdac6 and Sirt2 [12, 13]. We found no change in Atat1 expression. In contrast, we found a significant induction in Hdac6 and Sirt2. Our data suggest that reduction in acetylated MTs (long-lived, stable, and protected from mechanical strain) is mediated via tubulin deacetylase action.

Previous evidence shows that MTs stabilization reduces fibrosis after spinal cord injury in rodents [14], and MTs destabilization due to loss of α-tubulin acetylation is associated with TGF-β induced EMT in vitro [15]. Our study suggests that MTs destabilization due to increased α-tubulin with a reduction in α-tubulin acetylation may facilitate HSC activation and fibrosis. Immunofluorescence analysis found an increase in α-tubulin starts before fibrotic changes in *Atp7b*$^{-/-}$ mice in hepatocytes (primarily) and non-parenchymal liver cells at ~ 7 weeks whereas tubulin, along with desmin and SMA (markers of HSCs activation) expression is significantly increased at 20 weeks. RNA sequencing revealed that tubulin induction correlated positively with fibrotic markers (Spp1, Col1a2, Timp1, Loxl2, Vim, and Acta2) in *Atp7b*$^{-/-}$ mice and patients with WD. Additionally, we also found similar positive correlations of tubulin deacetylase with fibrosis in *Atp7b*$^{-/-}$ mice and a negative correlation with Atat1. An increase in Hdac6 activity without affecting its expression in response to TGF-β causes tubulin deacetylation, promotes cytoskeletal reorganization, and favors EMT in epithelial cell (MCF-10A, HME) lines [15]. RNA-seq data in *Atp7b*$^{-/-}$ mice liver revealed a significant upregulation in EMT biomarkers such as cadherins (E, N), β-catenin, Fsp1, vimentin, collagens, Zeb2 etc. in murine WD (**Suppl. Table 5**). So, MTs rearrangement in *Atp7b*$^{-/-}$ mice may promote EMT. Our findings highlight that MTs destabilization due to increased tubulin deacetylation via Hdac6, and Sirt2 contributes to HSC activation and fibrosis in the murine model of WD.

Our RNA-seq data revealed about a ~ 31-fold increase in tubulin alpha 8 (Tuba8) expression in *Atp7b*$^{-/-}$ mice liver which was hardly detectable in Het control (**Suppl. Figure 7**). Tuba8 is a marker of HSCs induced in murine NASH and expressed by transformed hepatocytes in HCC [27]. This finding suggests that Tuba8 induction is associated with fibrotic changes and should be explored as a promising marker in hepatic fibrosis in the future. Another study reported that tubulin beta 3 and 4 are involved in the early fibrotic changes via endothelial-mesenchymal transition (Endo-MT) in human microvascular endothelial (HMEC-1) cells [28]. These studies suggest the importance of early tubulin induction in fibrogenesis and are concordant with our observations in murine WD.

Elevated Cu induces kidney fibrosis by lysyl oxidase-mediated matrix crosslinking in vitro and in vivo fibrosis models [20]. Lysyl oxidase-like 2 (Loxl2) is a Cu-dependent enzyme and we observed a significant positive correlation between fibrotic marker Loxl2 and tubulin expression in mouse and human WD. In the CCl4-induced liver fibrosis murine model, MT acetylation prominently appeared in the fibroblast-like cells near the blood vessels [29]. However, they did not find any change in total α-tubulin including hepatocyte involvement, unlike our study. Previously, we reported that liver fibrosis in *Atp7b*$^{-/-}$ mice occurs via TGF-β and other signaling pathways. TGF-β signaling is mediated by canonical SMAD and non-canonical SMAD (MAPK and Rho GTPase-Rac/CDC42) signaling pathways in murine WD [3]. TGF-β signaling is important for cytoskeletal reorganization and EMT. In this study, we found a plausible mechanism of cytoskeletal reorganization and EMT in Cu-overloaded conditions. Hepatic cytoskeleton is altered in animal model of WD with age and we delineated the mechanism of α-tubulin dysregulation leading to MT destabilization in *Atp7b*$^{-/-}$ mice.

Conditional deletion of Atp7b only in hepatocytes has no tubulin induction and no fibrotic changes despite steatosis and Cu accumulation even at 45 weeks. This could be due to not having enough Cu overload-mediated oxidative

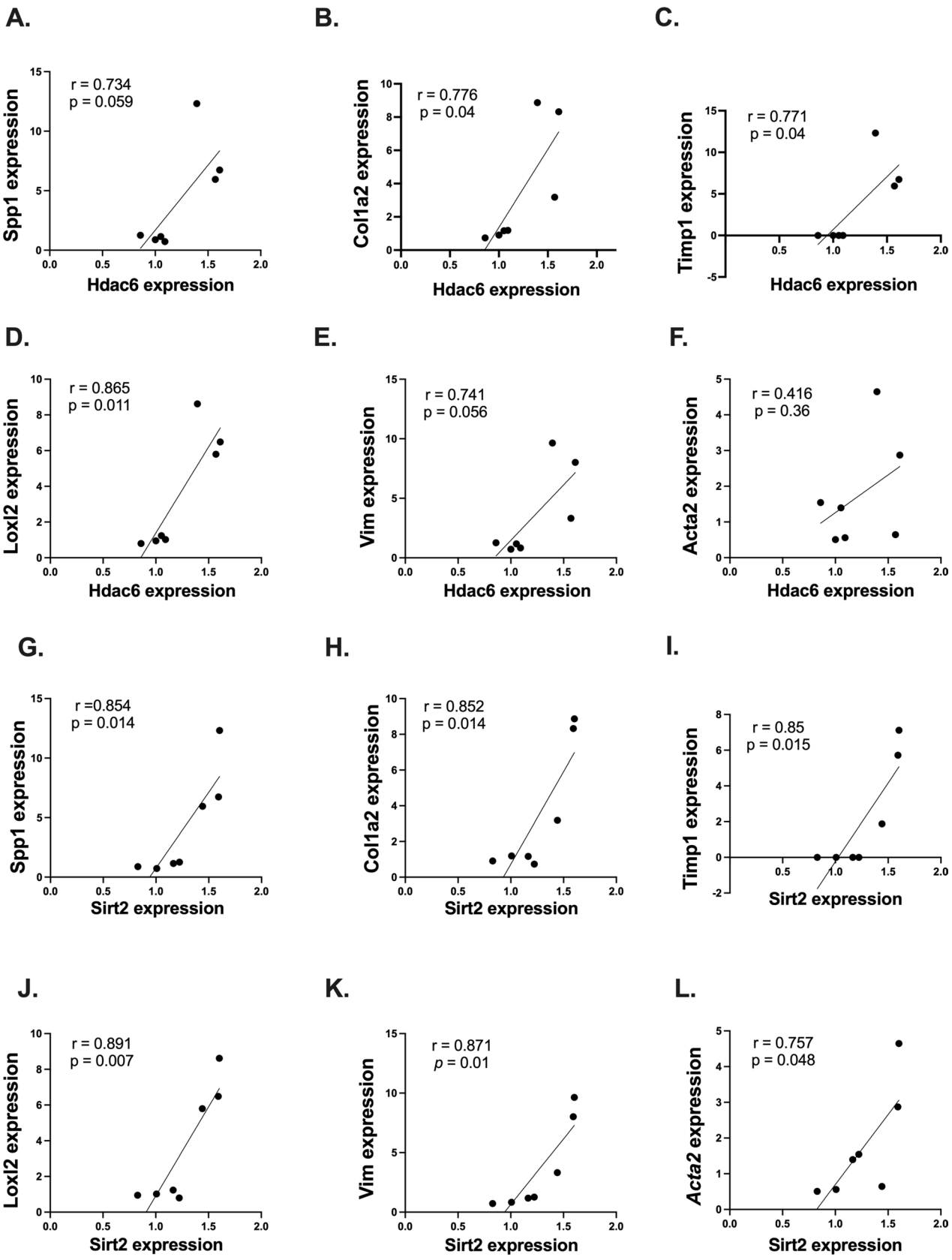
A.
r = 0.734
p = 0.059
Spp1 expression
Hdac6 expression
B.
r = 0.776
p = 0.04
Col1a2 expression
Hdac6 expression
C.
r = 0.771
p = 0.04
Timp1 expression
Hdac6 expression
D.
r = 0.865
p = 0.011
Loxl2 expression
Hdac6 expression
E.
r = 0.741
p = 0.056
Vim expression
Hdac6 expression
F.
r = 0.416
p = 0.36
Acta2 expression
Hdac6 expression
G.
r =0.854
p = 0.014
Spp1 expression
Sirt2 expression
H.
r = 0.852
p = 0.014
Col1a2 expression
Sirt2 expression
I.
r = 0.85
p = 0.015
Timp1 expression
Sirt2 expression
J.
r = 0.891
p = 0.007
Loxl2 expression
Sirt2 expression
K.
r = 0.871
p = 0.01
Vim expression
Sirt2 expression
L.
r = 0.757
p = 0.048
Acta2 expression
Sirt2 expression

◂**Fig. 5** Microtubule deacetylation positively correlated with fibrosis in *Atp7b*$^{-/-}$ mice. RNA expression (relative fold change) of fibrotic markers Spp1, Col1a2, Timp1, Loxl2, Vim, and Acta2 with respect to tubulin deacetylases Hdac6 **(A-F)** and Sirt2 **(G-L)** in the liver tissue from *Atp7b*$^{+/-}$ (n = 4) and *Atp7b*$^{-/-}$ (n = 3) mice at 20 weeks. Tubulin deacetylase induction was positively correlated with fibrosis markers upregulation in *Atp7b*.$^{-/-}$ mice liver. Pearson correlation coefficient (r) and p-value were calculated from Graph pad prism 10

stress, increased antioxidant defense, and normal Cu homeostasis in the non-parenchymal liver cells especially HSCs in *Atp7b*$^{\Delta Hep}$ mice [21, 25]. On the other hand, transcriptomics analysis in WD patient liver revealed a significant positive correlation between tubulin induction and fibrotic markers (Suppl. Figure 4). Though there were no significant changes in Atat1, Hdac6, and Sirt2 mRNA expression in the WD dataset, there was a trend of significant positive correlation between Sirt2 and fibrosis and negative correlation between Atat1 and fibrosis similar to murine WD.

Recent literature and publicly available transcriptomics reveal that there is a general trend of MTs gene upregulation in fibrosis. However, Hdac6 and Sirt2 essential for tubulin deacetylation and overall microtubules instability are differentially regulated in fibrotic conditions. A recent report in CCl_4 and TAA-induced liver fibrosis animal models demonstrated tubulin genes upregulation by 12 weeks of toxins exposure and significant down-regulation of tubulin concomitant with upregulation of Sirt3, Hdac5 in CCl_4 model and Sirt2, Sirt4, Sirt5, Sirt8 and Hdac8, Hdac10, Hdac11 in TAA model within 1–2 weeks following regression [30; Array express EMTAB-13804]. Another study reported that hepatocyte-specific Sirt2 deletion promotes hepatic fibrosis in CCl_4-treated mice highlighting the role of Sirt2 in hepatic fibrosis [31]. The renal fibrosis UUO model has more than ~ 2.37-fold increase in Tub1a and 1.6-fold increase in Hdac6 expression whereas Sirt2 expression was unchanged within 2-day ligation [32; GSE79443]. Hdac6 is induced in animal models of renal fibrosis [33] and cardiac fibrosis [34], and in human idiopathic pulmonary fibrosis [35]. Primary sclerosing cholangitis and or primary biliary cholangitis patients from grade 1 to 4 fibrosis progression induces Tub1a expression without Hdac6 and Sirt2 [36; https://zenodo.org/records/13990103]. Additionally, our recent study and other microarray data could not find change in Hdac6 expression at presymptomatic age at 12 weeks [37, 38] whereas upregulated in *Atp7b*$^{-/-}$ mice with established liver disease (at 20 weeks) in this study. Enzyme expression per se may not be changed rather Hdac6 and Sirt2 activity might be critical for regulating acetylation/deacetylation status and fibrogenesis.

In conclusion, we identified cytoskeletal system is altered in the WD liver, and a significant increase in α-tubulin expression is associated with its decreased acetylation resulting in MTs destabilization. The increase in α-tubulin protein is due to heightened transcription rate and MTs destabilization is due to Hdac6, Sirt2 mediated deacetylation. Our study shows that MTs instability-led cytoskeletal rearrangement in *Atp7b*$^{-/-}$ mice may promote EMT and induction of fibrotic markers positively correlated with α-tubulin in *Atp7b*$^{-/-}$ mice liver including WD patients. Tubulin deacetylation also positively correlated with fibrosis in murine WD (Fig. 6). No significant changes in MTs and fibrotic markers occur in hepatocyte-specific *Atp7b*$^{\Delta Hep}$ mice and before the

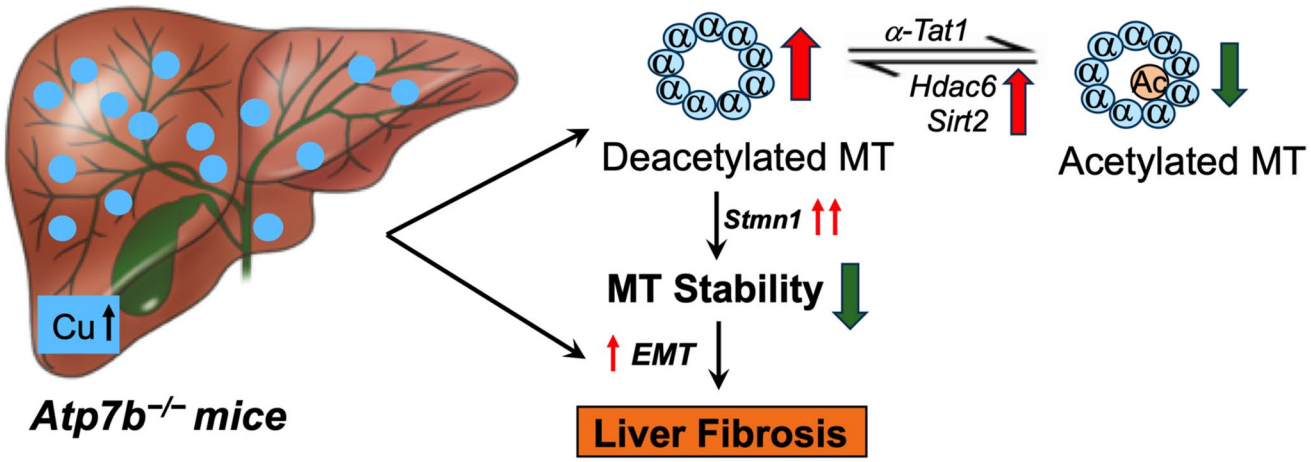

Fig. 6 Proposed model of hepatic microtubule destabilization facilitates liver fibrosis in the murine WD. In *Atp7b*$^{-/-}$ mice, hepatic cytoskeletal system is altered with a significant increase in α-tubulin expression is associated with its decreased acetylation resulting in MTs destabilization. MTs destabilization is mediated via tubulin deacetylases (Hdac6 and Sirt2) and Stmn1 induction. MTs instability-led cytoskeletal rearrangement in *Atp7b*$^{-/-}$ mice may promote EMT in Cu-overloaded conditions and induction of fibrotic markers positively correlated with MTs instability in *Atp7b*$^{-/-}$ mice liver including WD patients. Red arrow denotes the up-regulation and green arrow denotes the down-regulation

pathological onset in *Atp7b*$^{-/-}$ mice. Thus, these findings further illustrate that MTs destabilization is crucial to facilitate liver fibrogenesis and disease progression in WD.

Supplementary Information The online version contains supplementary material available at https://doi.org/10.1007/s00109-025-02535-y.

Acknowledgements We thank Dr. Abigael Muchenditsi for generating *Atp7b*$^{-/-}$ mice of C57BL/6 J background. We thank Prof. Svetlana Lutsenko for providing critical feedback and partial funding support. We thank Dr. Dominik Huster for performing Microarray in WD and control liver specimens. We thank Psomagen Inc, Rockville, MD, for performing RNA-Sequencing in *Atp7b*$^{-/-}$ and *Atp7b*$^{+/-}$ mice liver and basic dataset analysis. We also like to thank C. Conover Talbot, Jr. for helping with the microarray data analysis.

Author contributions Som Dev, James P. Hamilton conceived and designed the research. Som Dev and Yixuan Dong performed the research including material preparation, data collection. Som Dev, James P. Hamilton analyzed the data and wrote the paper. All authors read and approved the final manuscript.

Funding This work was partially supported by the National Institute of Health grant RO1- DK117396 to Dr. James P. Hamilton and Svetlana Lutsenko.

Data availability Data analyzed during the current study (generated in lab) are available at the Gene Expression Omnibus database (https://www.nlm.nih.gov/geo/) under accession numbers GSE174015 (mouse) and GSE197406 (human).

Declarations

Conflict of interest Patent: Targeting liver nuclear receptor as a treatment for WD; inventor: James P. Hamilton (PCT/US2015/054135 filed 10/7/2015). The author declares that they have no other competing interests.

References

1. Friedman SL (2003) Liver fibrosis-from bench to bedside. J Hepatol 38(Suppl 1):S38-53. https://doi.org/10.1016/s0168-8278(02)00429-4
2. Alkhouri N, Gonzalez-Peralta RP, Medici V (2023) Wilson disease: a summary of the updated AASLD Practice Guidance. Hepatol Commun 7(6):e0150. https://doi.org/10.1097/HC9.0000000000000150
3. Dev S, Muchenditsi A, Gottlieb A, Deme P, Murphy S, Gabrielson KL, Dong Y, Hughes R, Haughey NJ, Hamilton JP, Lutsenko S (2022) Oxysterol misbalance critically contributes to Wilson disease pathogenesis. Sci Adv 8:eadc9022. https://doi.org/10.1126/sciadv.adc9022
4. Huster D, Finegold MJ, Morgan CT, Burkhead JL, Nixon R, Vanderwerf SM, Gilliam CT, Lutsenko S (2006) Consequences of copper accumulation in the livers of the Atp7b-/- (Wilson disease gene) knockout mice. Am J Pathol 168:423–434. https://doi.org/10.2353/ajpath.2006.050312
5. Friedman SL (2008) Mechanisms of hepatic fibrogenesis. Gastroenterology 134:1655–1669. https://doi.org/10.1053/j.gastro.2008.03.003
6. Kisseleva T, Brenner D (2021) Molecular and cellular mechanisms of liver fibrosis and its regression. Nat Rev Gastroenterol Hepatol 18:151–166. https://doi.org/10.1038/s41575-020-00372-7
7. Cui X, Zhang X, Yin Q, Meng A, Su S, Jing X, Li H, Guan X, Li X, Liu S, Cheng M (2014) F-actin cytoskeleton reorganization is associated with hepatic stellate cell activation. Mol Med Rep 9:1641–1647. https://doi.org/10.3892/mmr.2014.2036
8. Shi Z, Rockey DC (2017) Upregulation of the actin cytoskeleton via myocardin leads to increased expression of type 1 collagen. Lab Invest 97:1412–1426. https://doi.org/10.1038/labinvest.2017.96
9. Westermann S, Weber K (2003) Post-translational modifications regulate microtubule function. Nat Rev Mol Cell Biol 4:938–947. https://doi.org/10.1038/nrm1260
10. Janke C, Montagnac G (2017) Causes and Consequences of Microtubule Acetylation. Curr Biol 27:R1287–R1292. https://doi.org/10.1016/j.cub.2017.10.044
11. Akella JS, Wloga D, Kim J, Starostina NG, Lyons-Abbott S, Morrissette NS, Dougan ST, Kipreos ET, Gaertig J (2010) MEC-17 is an alpha-tubulin acetyltransferase. Nature 467:218–222. https://doi.org/10.1038/nature09324
12. Hubbert C, Guardiola A, Shao R, Kawaguchi Y, Ito A, Nixon A, Yoshida M, Wang XF, Yao TP (2002) HDAC6 is a microtubule-associated deacetylase. Nature 417:455–458. https://doi.org/10.1038/nature09324
13. North BJ, Marshall BL, Borra MT, Denu JM, Verdin E (2003) The human Sir2 ortholog, SIRT2, is an NAD$^+$-dependent tubulin deacetylase. Mol Cell 11:437–444. https://doi.org/10.1016/s1097-2765(03)00038-8
14. Hellal F, Hurtado A, Ruschel J, Flynn KC, Laskowski CJ, Umlauf M, Kapitein LC, Strikis D, Lemmon V, Bixby J et al (2011) Microtubule stabilization reduces scarring and causes axon regeneration after spinal cord injury. Science 331:928–931. https://doi.org/10.1126/science.1201148
15. Gu S, Liu Y, Zhu B, Ding K, Yao TP, Chen F, Zhan L, Xu P, Ehrlich M, Liang T et al (2016) Loss of α-Tubulin Acetylation Is Associated with TGF-β-induced Epithelial-Mesenchymal Transition. J Biol Chem 291:5396–5405. https://doi.org/10.1074/jbc.M115.713123
16. Perrin LP, Roudeau S, Carmona A, Domart F, Petersen JD, Bohic S, Yang Y, Cloetens P, Ortega R (2017) Zinc and Copper Effects on Stability of Tubulin and Actin Networks in Dendrites and Spines of Hippocampal Neurons. ACS Chem Neurosci 8:1490–1499. https://doi.org/10.1021/acschemneuro.6b00452
17. Böhm KJ (2015) Elevated copper ion levels as potential cause of impaired kinesin-dependent transport processes. Arch Toxicol 89:565–572. https://doi.org/10.1007/s00204-014-1272-0
18. Lim CM, Cater MA, Mercer JF, La Fontaine S (2006) Copper-dependent interaction of dynactin subunit p62 with the N terminus of ATP7B but not ATP7A. J Biol Chem 281:14006–14014. https://doi.org/10.1074/jbc.M512745200
19. Polishchuk EV, Concilli M, Iacobacci S, Chesi G, Pastore N, Piccolo P, Paladino S, Baldantoni D, van IJzendoorn SC, Chan J

et al (2014) Wilson disease protein ATP7B utilizes lysosomal exocytosis to maintain copper homeostasis. Dev Cell 29:686–700. https://doi.org/10.1016/j.devcel.2014.04.033
20. Niu YY, Zhang YY, Zhu Z, Zhang XQ, Liu X, Zhu SY, Song Y, Jin X, Lindholm B, Yu C (2020) Elevated intracellular copper contributes a unique role to kidney fibrosis by lysyl oxidase mediated matrix crosslinking. Cell Death Dis 11:211. https://doi.org/10.1038/s41419-020-2404-5
21. Muchenditsi A, Talbot CC Jr, Gottlieb A, Yang H, Kang B, Boronina T, Cole R, Wang L, Dev S, Hamilton JP et al (2021) Systemic deletion of Atp7b modifies the hepatocytes' response to copper overload in the mouse models of Wilson disease. Sci Rep 11:5659. https://doi.org/10.1038/s41598-021-84894-3
22. Hamilton JP, Koganti L, Muchenditsi A, Pendyala VS, Huso D, Hankin J, Murphy RC, Huster D, Merle U, Mangels C et al (2016) Activation of liver X receptor/retinoid X receptor pathway ameliorates liver disease in Atp7B(-/-) (Wilson disease) mice. Hepatology 63:1828–1841. https://doi.org/10.1002/hep.28406
23. Schmittgen TD, Livak KJ (2008) Analyzing real-time PCR data by the comparative C(T) method. Nat Protoc 3:1101–1108. https://doi.org/10.1038/nprot.2008.73
24. Tang D, Chen M, Huang X, Zhang G, Zeng L, Zhang G, Wu S, Wang Y (2023) SRplot: A free online platform for data visualization and graphing. PLoS ONE 18:e0294236. https://doi.org/10.1371/journal.pone.0294236
25. Muchenditsi A, Yang H, Hamilton JP, Koganti L, Housseau F, Aronov L, Fan H, Pierson H, Bhattacharjee A, Murphy R et al (2017) Targeted inactivation of copper transporter Atp7b in hepatocytes causes liver steatosis and obesity in mice. Am J Physiol Gastrointest Liver Physiol 313:G39–G49. https://doi.org/10.1152/ajpgi.00312.2016
26. Akpolat N, Yahsi S, Godekmerdan A, Yalniz M, Demirbag K (2005) The value of alpha-SMA in the evaluation of hepatic fibrosis severity in hepatitis B infection and cirrhosis development: a histopathological and immunohistochemical study. Histopathology 47:276–280. https://doi.org/10.1111/j.1365-2559.2005.02226.x
27. Rein-Fischboeck L, Pohl R, Haberl EM, Zimny S, Neumann M, Eisinger K, Weiss TS, Krautbauer S, Buechler C (2017) Tubulin alpha 8 is expressed in hepatic stellate cells and is induced in transformed hepatocytes. Mol Cell Biochem 428:161–170. https://doi.org/10.1007/s11010-016-2926-4
28. Wawro ME, Sobierajska K, Ciszewski WM, Wagner W, Frontczak M, Wieczorek K, Niewiarowska J (2017) Tubulin beta 3 and 4 are involved in the generation of early fibrotic stages. Cell Signal 38:26–38. https://doi.org/10.1016/j.cellsig.2017.06.014
29. You E, Ko P, Jeong J, Keum S, Kim JW, Seo YJ, Song WK, Rhee S (2020) Dynein-mediated nuclear translocation of yes-associated protein through microtubule acetylation controls fibroblast activation. Cell Mol Life Sci 77:4143–4161. https://doi.org/10.1007/s00018-019-03412-x
30. Petrenko O, Königshofer P, Brusilovskaya K, Hofer BS, Bareiner K, Simbrunner B, Jühling F, Baumert TF, Lupberger J, Trauner M et al (2024) Transcriptomic signatures of progressive and regressive liver fibrosis and portal hypertension. iScience 27:109301. https://doi.org/10.1016/j.isci.2024.109301
31. Yang S, Yang G, Wang X, Xiang J, Kang L, Liang Z (2023) SIRT2 alleviated renal fibrosis by deacetylating SMAD2 and SMAD3 in renal tubular epithelial cells. Cell Death Dis 14:646. https://doi.org/10.1038/s41419-023-06169-1
32. Arvaniti E, Moulos P, Vakrakou A, Chatziantoniou C, Chadjichristos C, Kavvadas P, Charonis A, Politis PK (2016) Whole-transcriptome analysis of UUO mouse model of renal fibrosis reveals new molecular players in kidney diseases. Sci Rep 6:26235. https://doi.org/10.1038/srep26235
33. Chen X, Yu C, Hou X, Li J, Li T, Qiu A, Liu N, Zhuang S (2020) Histone deacetylase 6 inhibition mitigates renal fibrosis by suppressing TGF-β and EGFR signaling pathways in obstructive nephropathy. Am J Physiol Renal Physiol 319:F1003–F1014. https://doi.org/10.1152/ajprenal.00261.2020
34. Tao H, Yang JJ, Hu W, Shi KH, Li J (2016) HDAC6 Promotes Cardiac Fibrosis Progression through Suppressing RASSF1A Expression. Cardiology 133:18–26. https://doi.org/10.1159/000438781
35. Saito S, Zhuang Y, Shan B, Danchuk S, Luo F, Korfei M, Guenther A, Lasky JA (2017) Tubastatin ameliorates pulmonary fibrosis by targeting the TGFβ-PI3K-Akt pathway. PLoS ONE 12:e0186615. https://doi.org/10.1371/journal.pone.0186615
36. Laschtowitz A, Lindberg EL, Liebhoff AM, Liebig LA, Casar C, Steinmann S, Guillot A, Xu J, Schwinge D, Trauner M et al (2024) Liver transcriptome analysis reveals PSC-attributed gene set associated with fibrosis progression. JHEP Reports 7:101267
37. Gottlieb A, Dev S, DeVine L, Gabrielson KL, Cole RN, Hamilton JP, Lutsenko S (2022) Hepatic Steatosis in the Mouse Model of Wilson Disease Coincides with a Muted Inflammatory Response. Am J Pathol 192:146–159. https://doi.org/10.1016/j.ajpath.2021.09.010
38. Wooton-Kee CR, Robertson M, Zhou Y, Dong B, Sun Z, Kim KH, Liu H, Xu Y, Putluri N, Saha P et al (2020) Metabolic dysregulation in the *Atp7b*$^{-/-}$ Wilson's disease mouse model. Proc Natl Acad Sci U S A 117:2076–2083. https://doi.org/10.1073/pnas.1914267117